Open Archive TOULOUSE Archive Ouverte (OATAO)

OATAO is an open access repository that collects the work of Toulouse researchers and makes it freely available over the web where possible.

This is an author-deposited version published in : http://oatao.univ-toulouse.fr/
Eprints ID : 14016

Any correspondance concerning this service should be sent to the repository administrator: staff-oatao@listes-diff.inp-toulouse.fr

DFT study of the solubility of hydrogen and carbon in Ni_3Nb-$D0_a$ and Ni_3Nb-$D0_{22}$ systems

Damien Connétable [*], Florian Galliano, Grégory Odemer, Christine Blanc, Éric Andrieu

CIRIMAT, UMR 5085, CNRS-UPS-INP, École Nationale d'Ingénieurs en Arts Chimiques et Technologiques (ENSIACET), 4, allée Émile Monso, BP 44362, F-31030 Toulouse Cedex 4, France

A B S T R A C T

The influence of the local environment on C and H atoms was investigated in Ni_3Nb-$D0_a$ (space group 59) and Ni_3Nb-$D0_{22}$ (space group 139) crystals. The interstitial positions of these atoms and their solubility energies were studied by analyzing the results of first-principles calculations based on density functional theory. The results were compared with those obtained in pure and Nb alloyed fcc Ni. For C atoms, several possible interstitial sites were found, but only one (per structure) is slightly more stable than the others: the *4d* sites for $D0_a$ and the *4c* sites for $D0_{22}$. The C atom is slightly soluble and its solubility energy is equivalent in the two intermetallic structures: approximately equal to 1.06 eV, which is significantly larger than in fcc Ni (0.55 eV). In the case of hydrogen, other interstitial sites were identified: the *4e* positions for both $D0_a$ and $D0_{22}$. The solubility energy in $D0_a$ (approximately 0.12 eV, without the zero-point energy correction) was found to be smaller than that in $D0_{22}$ (0.17 eV) but larger than that in nickel (0.09 eV). With the zero-point energy correction, the solubility in both Ni_3Nb alloys is therefore equivalent. These results were finally used to assess the fraction of light elements in Ni_3Nb relative to that in fcc Ni and that in Ni doped Nb.

1. Introduction

Alloy 718 is an Ni-based, Nb-rich superalloy whose excellent mechanical properties are, in large part attributable to the precipitation of Ni_3Nb phases: δ precipitates (with a $D0_a$ structure) and γ'' precipitates (with a $D0_{22}$ structure). Moreover, strong reactions of alloying elements with carbon to form carbides (W—C, Cr—C) are used to strengthen the alloy by controlling the grain size during the elaboration process or to improve the high-temperature mechanical properties by reducing grain-boundary slippage [1–3].

Alloy 718 is widely used in aqueous or H_2-rich environments for high-temperature applications, even though, like many Ni-based alloys, it is susceptible to hydrogen embrittlement [4–10] and exhibits high solubility in hydrogen. Previous studies have suggested that the Nb atoms exert some influence on the hydrogen solubility of these alloys [11,12]. In addition, some studies [9,10,13] have identified potential hydrogen traps in alloy 718: niobium-rich phases such as carbides and δ and γ'' precipitates. These traps remain active at moderate temperatures of up to 300 °C. However, the exact role of δ and γ'' precipitates in hydrogen trapping is not yet well understood. Indeed hydrogen can be diluted and become trapped in these precipitates or at their interfaces with the Ni-rich matrix. There are no data available regarding the interaction between hydrogen and Ni_3Nb structures at the atomic scale.

The kinetics for the precipitation of Ni_3Nb phases depends strongly on the C content in the alloy. The interaction of the C and H content in the presence or absence of Ni_3Nb precipitates, i.e., in the presence or absence of an Nb-rich solid solution, remain unknown. We expect that, the solubility of the interstitials and their diffusion properties, particularly those of C and H atoms dissolved in the metal base structure, both may vary depending on the Nb content in the solid solution. Although the effects of the Nb content on the diffusion may be difficult to evaluate, *ab initio* calculations can help to determine the content of interstitials in Ni_3Nb.

The results presented in this study provide information regarding the differences in H and C solubility between the Ni matrix and Ni_3Nb structures. Although the structures of Ni_3Nb are well known [14–18], the interstitial sites and the solubility energies of light elements in such structures are currently unknown. Therefore, results concerning the solubility of C and H atoms in these structures were obtained using first-principles calculations based on Density Functional Theory and including the zero-point-energy correction for the H atoms. In addition, the effect of the Nb content in the nickel solid solution on the H solubility was investigated.

* Corresponding author. Tel.: +33 5 34 32 34 10.
   E-mail address: damien.connetable@ensiacet.fr (D. Connétable).

In the next section of the paper, *ab initio* calculations are presented. Then, in the following section, the ground-state properties of Ni_3Nb structures are summarized. In the two subsections, the interstitial positions that C and H atoms can occupy in the $D0_a$ and $D0_{22}$ structures are presented. Finally, assessments of the fractions of C and H present in Ni_3Nb relative to the Ni matrix and the Nb—C/H interactions in nickel are proposed.

2. Methods

Calculations were performed using the Vienna *ab initio* simulation package (VASP) [19]. The Kohn–Sham equations were solved by using the projector augmented-wave (PAW) method [20] to describe the electron–ion interactions and using the Perdew–Wang (PW 91) approximation [21] for the exchange and correlation functionals. Because no magnetism was found in the Ni_3Nb structures, the magnetic moments were not included in the calculations (see below). In the case of the simulations of fcc Ni, magnetic effects were taken into account. The cut-off energy was set to 500 eV, and $20 \times 20 \times 10$ and $20 \times 20 \times 20$ **k**-mesh grids were used to sample the reciprocal Brillouin zone of the primitive cells of the Ni_3Nb-$D0_{22}$ and Ni_3Nb-$D0_a$ structures, respectively. Lattice relaxations were introduced by means of a conjugate-gradient algorithm. These parameters provided accurate energies (less 3 meV/atom); many tests were performed to validate the choices of parameters.

Different configurations were considered depending on the specifics of the crystallography of each phase to evaluate the solubility energies and to determine the preferred positions. In the following discussion, we present only results related to the interstitial configurations because, as is the case in fcc Ni, the substituted configurations in Ni_3Nb (results not reported here) have larger solubility energies than the interstitial sites. The solubility energies in the interstitial sites ($E^{sol}[X]$) were calculated as follows:

$$E^{sol}[X] = E_o[X + Ni_3Nb] - E_o[Ni_3Nb] - \mu^o[X_{ref}] \quad (1)$$

where $E_o[X + Ni_3Nb]$ and $E_o[Ni_3Nb]$ are the energies of the system with and without any impurity in an interstitial site, respectively. $\mu^o[X_{ref}]$ corresponds to the potential energy (per atom) of the reference state. For H and C atoms (the H_2 molecule and diamond, respectively) and the Ni and Nb reference states (fcc and bcc structures), the ground-state properties found in this manner are in excellent agreement with the literature (see Refs. [22,23]).

3. Ni_3Nb systems

Ni_3Nb-$D0_a$ has an orthorhombic structure with eight atoms in the primitive cell (*Pmmn*, space group 59). The nickel atoms are located in the *2b* $(0, 1/2, z = 0.317)$ and *4f* $(x = 0.249, 0, z = 0.159)$ Wyckoff positions, and the Nb atoms are in the *2a* $(0, 0, z = 0.674)$ positions. In the case of Ni_3Nb-$D0_{22}$, a tetragonal structure (*I4/mmm*, space group 139), the Ni atoms are located in the *4d* $(0, 1/2, 1/4)$ and *2b* $(0, 0, 1/2)$ positions, and the Nb atoms are in the *2a* $(0, 0, 0)$ positions.

Table 1 presents a comparison of the optimized and experimental lattice parameters and the formation energies of the two structures. The results (lattice parameters and atomic positions) obtained in this study are in excellent agreement with those reported in the experimental [14,15] and theoretical [16–18] literature; the discrepancy is less than 1%. The structures do not exhibit any magnetic behavior, even when interstitial elements are inserted into the networks (several tests were performed to confirm this claim). The $D0_a$ structure is slightly more stable than $D0_{22}$, as indicated in the literature.

Table 1
Lattice parameters (in units of Å), magnetic moments (μ in units of μ_B) and cohesive energies (E_{coh} in units of meV/atom) of the Ni_3Nb-$D0_a$ and Ni_3Nb-$D0_{22}$ structures.

	a_o	b_o	c_o	E_{coh}	μ
$D0_a$	5.128[a]	4.265	4.570	−304	0
	5.117[b]	4.254	4.551	−314	0
	5.114[c]	4.244	4.53	–	0
$D0_{22}$	3.646[a]	–	7.508	−296	0
	3.643[b]	–	7.484	−308	0
	3.62[d]	–	7.41	–	0

[a] PW91, VASP present work.
[b] PBE, VASP [17].
[c] Expt. [14].
[d] Expt. [15].

4. Solubility in $D0_a$

In the case of the Ni_3Nb-$D0_a$ system, $2 \times 2 \times 2$ supercells were used to determine the optimized positions for H and C atoms and to compute their solubility energies. The mean distance between two adjacent impurities was equal to approximately 8.5 Å. Fifteen different (non-equivalent) initial positions were considered, and all configurations were fully relaxed. The same initial positions were used for both elements. After relaxation, only a few non-equivalent positions were identified, i.e., 5 and 7 for the C and H atoms, respectively. All positions are illustrated Figs. 1 and 2. The optimized positions are listed in Table 2. Table 2 also presents the solubility energies of the optimized configurations.

For H atoms, several configurations, i.e., seven final positions (see Fig. 2) were obtained. Nevertheless, there is only one preferred site for H atoms: the *4e* position $(0, 0.49, 0.36)$. Its solubility energy is significantly lower (0.12 eV) than those of the other configurations (>0.31 eV).

For H atoms the zero-point energy (ZPE) plays a significant role in the solubility energy. The H frequencies and, therefore, the ZPE (using the $\sum_i \hbar\omega_i/2$ formula at 0 K) were computed for the most stable configuration. The H frequencies were calculated only to first order, neglecting the vibrations of the network. They were computed using a frozen-mode approach, in which the relative displacements were equal to 0.01. We obtained three frequencies of 1423, 1239 and 798 cm^{-1}; the ZPE is thus equal to approximately 210 meV. When the ZPE of the H_2 molecule (approximately 134 meV) is taken into account, the vibrational solubility energy is equal to 77 meV for H atoms in the $D0_a$ structure. *In fine*, the solubility enthalpy of H atoms in $D0_a$ is equal to approximately 0.19 eV.

For C atoms, five configurations were found. The *4d* position $(1/4, 1/4, 1/2)$ was determined to be the most stable position. Its
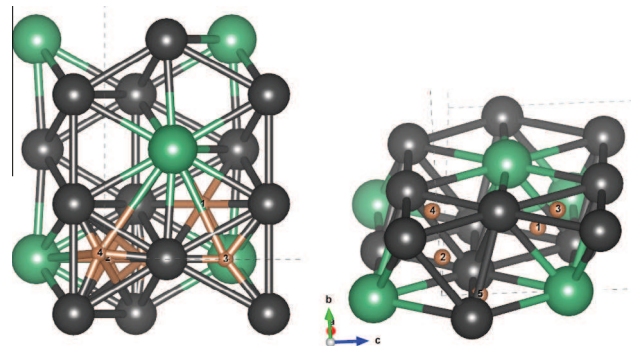
Fig. 1. Schematic illustration of the optimized configurations for C atoms in Ni_3Nb-$D0_a$ (the entire supercell is not shown). Ni atoms are depicted in gray. The different numbers correspond to the different final positions.
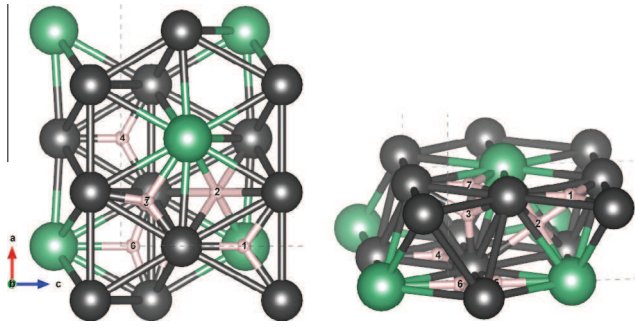
Fig. 2. Schematic illustration of the optimized configurations for H atoms in Ni$_3$Nb-D0$_a$.

Table 2
Optimized configurations for C and H atoms in Ni$_3$Nb-D0$_a$. The solubility energies (E^{sol}[X], in units of eV) of the various interstitial positions are listed. The optimized atomic positions, in relative coordinates (in the primitive cell), are also given. The numbers correspond to the positions shown in Figs. 1 and 2. In the case of H atoms, the zero-point-energy (ZPE, in units of meV) is given.

Position		(x,y,z)	E^{sol}[X]	ZPE
Hydrogen				
4e	(1)	$(0, 0.49, 0.36)$	0.12	210
4d	(2)	$(1/4, 1/4, 1/2)$	0.31	–
8g	(3)	$(0.20, 0.34, 0.13)$	0.38	–
2b	(4)	$(0, 1/2, 0.01)$	0.43	–
2a	(5)	$(0, 0, 0.25)$	0.56	–
2a	(6)	$(0, 0, 0.06)$	0.60	–
4f	(7)	$(0.21, 0, 0.14)$	0.70	–
Carbon				
4d	(1)	$(1/4, 1/4, 1/2)$	1.06	104
4e	(2)	$(0, 0.27, 0.01)$	1.18	108
2b	(3)	$(0, 1/2, 0.38)$	1.63	–
2a	(4)	$(0, 0, 0.19)$	2.22	–
4f	(5)	$(0.47, 0, 0.03)$	2.34	–

solubility energy is equal to approximately 1.06 eV. In contrast to the H case, there is a second site (not equivalent to the previous one) of comparable energy: the *4e* position (1.18 eV). We also computed the ZPE for these configurations. We found 104 and 108 meV, respectively. For the reference state (C diamond), the ZPE at 0K is approximately equal to 178 meV [24]. The vibrational enthalpy is thus small, -74 and -70 meV, and does not change significantly the value of the formation enthalpy (the same comment could be done in the following for C atoms in solid solution in fcc Ni and Ni$_3$Nb-D0$_{22}$).

5. Solubility in D0$_{22}$

To study the behavior of C and H atoms in D0$_{22}$, $2 \times 2 \times 1$ supercells were used. The smallest distance between defects in all directions was always larger than 7 Å. The distances between neighboring images were sufficient to neglect the interactions between them. Some simulations were performed using larger supercells ($3 \times 3 \times 2$) to test the accuracy of the simulations, and no significant difference was found in the final energies (approximately 15 meV; values are listed in Table 3, indicated with *).

As in the case of D0$_a$, various initial configurations were considered, but only a few optimized sites were identified in D0$_{22}$ (considering the symmetries of the crystal). The results of the simulations are summarized in Table 3.

For H atoms, five different configurations were obtained, with energies varying from 0.17 to 1.53 eV, depending on the site. Two additional specific configurations were also tested, (6) $(1/4, 1/4, 3/8)$ and (7) $(1/4, 1/4, 1/8)$ (see Fig. 3), but after relaxation,

Table 3
Solubility energies (E^{sol}, in units of eV) of the various optimized interstitial positions identified in Ni$_3$Nb-D0$_{22}$. In the case of H atoms, the zero-point energy (in units of meV) is listed. The atomic positions and Wyckoff positions are also listed.

Position		(x,y,z)	E^{sol}[X]	ZPE
Hydrogen				
4e	(1)	$(0, 0, 0.28)$	0.17/0.16[a]	141
4c	(2)	$(1/2, 0, 0)$	0.22/0.24[a]	165
16m	(3)	$(0.32, 0.32, 0.15)$	0.35	–
8f	(4)	$(1/4, 1/4, 1/4)$	0.68	–
16m	(5)	$(0.22, 0.22, 0.15)$	1.53	–
Carbon				
4c	(1)	$(1/2, 0, 0)$	1.05/1.05[a]	113
4e	(2)	$(0, 0, 0.26)$	1.43	–
8f	(3)	$(1/4, 1/4, 1/4)$	2.24	–
8h	(4)	$(0.25, 0.25, 0)$	5.10	–

[a] Values computed using $3 \times 3 \times 2$ supercells.

both converged toward a configuration that was equivalent to the (3) case.

The most stable configuration corresponds to the *4e* positions $(0, 0, 0.28)$, with a solubility energy of 0.17 eV. The second most stable configuration has an energy of 0.22 eV. The ZPE was computed for these two configurations in the same manner as for D0$_a$. For the first configuration, we obtained three non-equivalent frequencies, 204, 82 and 44 meV (1648, 666, and 353 cm^{-1}). These results indicate that the ZPE is equal to 141 meV. For the second configuration, the frequencies were found to be 129, 77 and 75 meV (1041, 621 and 598 cm^{-1}), yielding a ZPE value of 165 meV. Finally, when the ZPE of H$_2$ is taken into account, the formation enthalpies for the most stable and second most stable configurations are equal to approximately 0.18 and 0.25 eV, respectively.

In the case of C atoms, the preferred sites are the *4c* (1.05 eV) and *4e* positions (1.43 eV). As in the case of the H atom, configurations (5) and (6) were tested, but the final position was always (2). It was thus determined that the solubility energy of the preferred site is the same as in D0$_a$.

6. Discussion

Robertson has noted [11] that for a given chemical composition, the solubility of H atoms in a nickel-based solid solution enriched with niobium strongly depends on the location of the niobium, i.e., a substitutional position or an intermetallic phase. In the case of
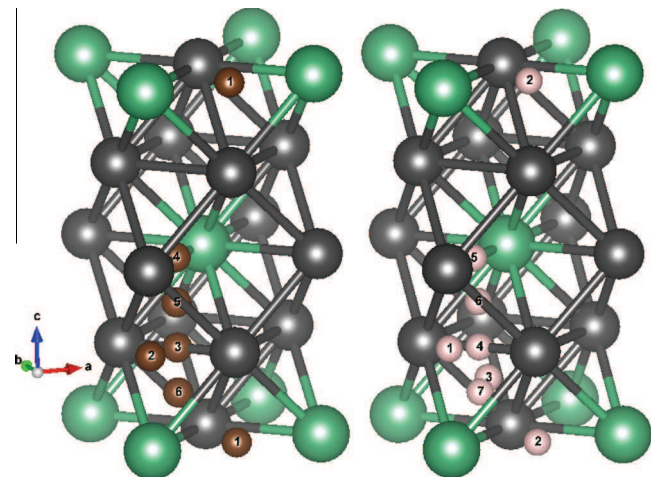
Fig. 3. Schematic illustration of the optimized configurations of C (left) and H (right) atoms in Ni$_3$Nb-D0$_{22}$ phases in one unit cell. Ni atoms are depicted in gray.

alloy 718, it has been demonstrated that, two metallurgical states that leads to Nb atoms that exists exclusively in solid solution and the state that leads to Nb atoms forming Ni_3Nb precipitates, do not dissolve similar amounts of H content as does pure nickel. Our DFT simulations on $D0_a$ and $D0_{22}$ can be used to analyze and interpret these experimental findings. Therefore, previous results were compared with DFT-based results concerning the solubility of H in pure and alloyed fcc-nickel. The comparison was also performed for carbon.

Using the same DFT approach presented in Refs. [23,25], one finds that the solubility energy of C in nickel is equal to 0.57 eV (2.20 eV) for the octahedral (tetrahedral) site and that, in the case of H atoms, the solubility energy for the octahedral (tetrahedral) site is approximately equal to 88 meV (311 meV) [22,26]. The H solubility energy, including the ZPE correction, is thus equal to 0.100 eV (0.411 eV) in fcc Ni.

Based on these values, the fraction of H/C atoms present in the precipitates was assessed, neglecting the segregation to the interface. To first order, the fraction F of X elements present in Ni_3Nb relative to the Ni matrix can be written as:

$$F \propto C(Ni_3Nb) \exp\left(-\frac{\Delta E^s[X]}{k_B T}\right) \propto C(Ni_3Nb)G \qquad (2)$$

where $\Delta E^s[X] = E^{sol}[X,Ni_3Nb] - E^{sol}[X,Ni]$, and $C(Ni_3Nb)$ is the precipitate content. For H atoms, $\Delta E^s[H] \approx 0.09$ eV, and this value is approximately 0.5 eV in the case of C atoms. δ and γ'' precipitates cannot be considered to be traps at low temperatures.

For a more thorough analysis, the influence of Nb atoms on the H/C solubility in nickel was studied. One Nb atom (Nb atoms are located in substitution sites in fcc Ni, see [27]) was substituted into an Ni supercell (in $2 \times 2 \times 2$, $3 \times 3 \times 3$ and $4 \times 4 \times 3$ supercells). Then, the X—Nb interactions (where X=C or H) were analyzed based on the X—Nb distance. The solubility energy was computed using the energy of the supercell with the Nb atom as the reference state ($E_o[(n-1) \cdot Ni + Nb]$), i.e.,

$$E^{sol}[X] = E_o[(n-1) \cdot Ni + Nb + X] - E_o[(n-1) \cdot Ni + Nb] - \mu^o[X_{ref}] \qquad (3)$$

The results are presented in Table 4.

In the case in which an H atom is located in the 1NN tetrahedral position, the optimized position relaxes to the octahedral 2NN site; the other tetrahedral configurations were not found to be energetically favored (data not reported here), as in the case of the ideal structure without any Nb atoms. In the octahedral sites, the 2NN–4NN configurations were found to have lower solubility

energies than in pure nickel, whereas the 1NN configuration was found to be energetically unfavorable. The ZPE correction to the 2NN solubility is low, approximately 10 meV.

It can be deduced that when the Nb content increases (up to 3 at%), the H solubility energy decreases. It was also found that the solubility of H atoms in Nb-alloyed Ni should slightly increase in the matrix, which is in qualitative agreement with the experimental results [11].

The Nb-rich region should trap more H atoms than the other regions. During the precipitation of Ni_3Nb, hydrogen atoms do not segregate into precipitates, but because there is always a small amount of Nb present in the matrix, the solubility energy is always lower than in pure nickel. Similar results and analysis apply in the case of the C atoms.

7. Conclusion

All possible interstitial sites for H and C atoms were analyzed in detail in the Ni_3Nb-$D0_a$ and Ni_3Nb-$D0_{22}$ structures.

The solubility energies for C atoms are equivalent in the two systems, approximately equal to 1.05 eV, which is significantly higher than the solubility energy in pure fcc Ni. C atoms should not segregate into these precipitates.

In the case of H atoms, different interstitial sites were identified. As in the case of carbon, the solubility energies in both Ni_3Nb structures are similar when the ZPE correction (0.19 eV) is included. This solubility energy is slightly larger than that in pure nickel (0.09 eV).

Based on these results and at study of X—Nb interactions, the evolution of the H content in Ni-based superalloys was qualitatively explained: when Nb atoms are present in a solid solution, the H content increases, and Ni_3Nb precipitates can dissolve only a low concentration of H atoms. Although the H (or C) solubility energy is higher in Nb—Ni crystals than in pure nickel, indicating that these elements should be slightly soluble in Ni_3Nb precipitates, Nb atoms in solid solution favor H solubility, which result is in agreement with various experimental observations. The volume in which hydrogen can be dissolved is reduced by the volume ratio of the precipitates.

Acknowledgments

Table 4
Solubility (E^{sol}, in units of eV) of the X—Nb clusters depending to the X—Nb distance (d(X—Nb), in units of Å), for various Nb content (in units of at%).

		$d(X—Nb)$	$E^{sol}[X]$			ZPE
H	in octa	–	0.08			145
C	in octa	–	0.57			114
Nb	content		3%	1%	0.5%	–
H	1NN	2.06	0.10	0.17	0.20[a]	160
	2NN	3.08	0.01	0.05	0.03[a]	143
	3NN	3.96	0.01	0.05	–	148
	4NN	5.29	–	0.06	–	–
	5NN	5.85	–	–	0.04[a]	–
C	1NN	2.18	0.69	0.93	0.94[a]	–
	2NN	3.13	0.34	0.48	0.49[a]	–
	3NN	3.99	0.33	0.48	–	–
	4NN	5.31	–	0.49	–	–
	5NN	5.86	–	–	0.49[a]	–

[a] Results obtained using $\times 4 \times 3$ supercells.

References

[1] G. Sabol, R. Stickler, Microstructure of nickel-based superalloys-review article, Phys. Status Solidi 39 (1969) 11.

[2] A. Jena, M. Chaturvedi, The role of alloying elements in the design of nickel-base superalloys, J. Mater. Sci. 19 (1984) 3121.

[3] G. Smith, S. Patel, The role of niobium in wrought precipitation-hardened nickel-base alloys, in: E.A. Loria (Ed.), Proceedings of Superalloys 718, 625, 706 and Various Derivatives 2005, TMS, 2005, pp. 135.

[4] J. Chene, A. Brass, Role of temperature and strain rate on the hydrogen-induced intergranular rupture in alloy 600, Metall. Mater. Trans. A 35 (2004) 457–464.

[5] D.M. Symons, The effect of hydrogen on the fracture toughness of alloy X-750 at elevated temperatures, J. Nucl. Mater. 265 (1999) 225–231.

[6] P. Hicks, C. Altstetter, Internal hydrogen effects on tensile properties of iron- and ni-base superalloys., Metall. Mater. Trans. A 21 (1990) 365–372.

[7] L. Fournier, D. Delafosse, T. Magnin, Cathodic hydrogen embrittlement in alloy 718, Mater. Sci. Eng. A 269 (1999) 111–119.

[8] P. Hicks, C. Altstetter, Hydrogen-enhanced cracking of superalloys, Metall. Trans. A 23 (1992) 237–249.

[9] L. Liu, C. Zhai, C. Lu, W. Ding, A. Hirose, K.F. Kobayashi, Study of the effect of δ phase on hydrogen embrittlement of inconel 718 by notch tensile tests, Corros. Sci. 47 (2005) 355–367.

[10] L. Liu, K. Tanaka, A. Hirose, K.F. Kobayashi, Effects of precipitation phases on the hydrogen embrittlement sensitivity of inconel 718, Sci. Technol. Adv. Mater. 3 (2002) 335–344.

[11] W. Robertson, Hydrogen permeation and diffusion in inconel 718 and incoloy 903, Metall. Trans. A 8 (1977) 1709–1712.

[12] F. Galliano, E. Andrieu, C. Blanc, J.-M. Cloué, D. Connétable, G. Odemer, Effect of trapping and temperature on the hydrogen embrittlement susceptibility of alloy 718, Mater. Sci. Eng. A (submitted for publication).

[13] B. Pound, The effect of aging on hydrogen trapping in precipitation-hardened alloys, Corros. Sci. 42 (2000) 1941–1956.

[14] T. Fang, S. Kennedy, L. Quan, T. Hicks, J. Phys.: Condens. Matter. 4 (1992) 2405.

[15] R. Cozer, A. Pineau, Metall. Trans. A 4 (1973) 47.

[16] Y. Cao, J. Zhu, Z. Nong, X. Yang, Y. Liu, Z. Lai, First-principles studies of the structural, elastic, electronic and thermal properties of ni_3nb, Comput. Mater. Sci. 77 (2013) 208–213.

[17] D. Connétable, M. Mathon, J. Lacaze, First principle calculations of fe–nb–ni–cr systems, Calphad 35 (2011) 588. http://dx.doi.org/10.1016/j.calphad.2011.09.004.

[18] S. Dai, W. Liu, First-principles study on the structural, mechanical and electronic properties of δ and γ'' phases in inconel 718, Comput. Mater. Sci. 49 (2010) 414–418.

[19] G. Kresse, J. Hafner, Phys. Rev. B47 (1993) 558.

[20] G. Kresse, D. Joubert, Phys. Rev. B59 (1999) 1758.

[21] Y. Wang, J.P. Perdew, Phys. Rev. B44 (1991) 13298.

[22] D. Connétable, Y. Wang, D. Tanguy, Segregation of hydrogen to defects in nickel using first-principle calculations: the case of self-interstitials and cavities, J. Alloys Compd, 2014 (accepted for publication).

[23] D. Connétable, E. Andrieu, D. Monceau, Ab initio study of impurities and defects in fcc-nickel, Computational Materials Science (submitted for publication).

[24] D. Connétable, First principle calculations of carbon clathrates: a comparison with silicon and germanium clathrates, Phys. Rev. B82 (2010) 075209, http://dx.doi.org/10.1103/PhysRevB.83.035206.

[25] D. Siegel, J. Hamilton, First principles study of solubility diffusion and clustering of C in NI, Phys. Rev. B68 (2003) 094105.

[26] E. Wimmer, W. Wolf, J. Sticht, P. Saxe, C. Geller, R. Najafabadi, G. Young, Temperature dependent diffusion coefficients from ab initio computations: H d and t in nickel., Phys. Rev. B77 (2008) 134305.

[27] D. Connétable, B. Ter-Ovanessian, E. Andrieu, Diffusion and segregation of niobium in fcc-nickel, J. Phys.: Condens. Matter 24 (2012) 095010, http://dx.doi.org/10.1088/0953-8984/24/9/095010.